

Journal of
Mechanics of
Materials and Structures

**A DISPLACEMENT POTENTIAL-BASED NUMERICAL SOLUTION
FOR ORTHOTROPIC COMPOSITE PANELS
UNDER END MOMENT AND SHEAR LOADING**

S. K. Deb Nath and S. Reaz Ahmed

Volume 4, N^o 6

June 2009



mathematical sciences publishers

A DISPLACEMENT POTENTIAL-BASED NUMERICAL SOLUTION FOR ORTHOTROPIC COMPOSITE PANELS UNDER END MOMENT AND SHEAR LOADING

S. K. DEB NATH AND S. REAZ AHMED

The elastic behavior of an orthotropic composite panel is analyzed under the influence of an end moment as well as shear loading. The panel is rigidly fixed at one of its ends, and the fibers are assumed to be directed along its length. An efficient finite difference computational scheme, based on the displacement potential formulation, is used to analyze the present mixed boundary value elastic problem. The effects of several important issues, for example, the panel aspect ratio, edge stiffening, and fiber reinforcement, on the elastic field are investigated. Solutions are presented mainly in the form of graphs and the predicted deformed shape. Finally, the reliability and superiority of the present computational scheme is discussed in comparison to the corresponding finite element predictions.

A list of symbols can be found on page 1003.

1. Introduction

The strength-to-weight ratio of a fiber reinforced composite material is usually higher than that of the corresponding isotropic material. The use of composite materials is increasing day by day, particularly to satisfy the demand for lightweight structures. The use of composite panels in the construction of engineering structures, for example, aircraft, is quite extensive. It is known that the mechanical properties, such as strength and toughness of a fiber reinforced composite, differ significantly from those of an isotropic material and eventually play an important role in defining the state of stress and deformation of the structural component under loading.

Stress analysis has now become a classical subject in the field of solid mechanics. However, stress analysis problems are still being examined with improved sophistication with respect to the methods of analysis [Conway et al. 1951; Chow et al. 1953; Krishna Murty 1984; Suzuki 1986; Durelli and Ranganayakamma 1989; Hardy and Pipelzadeh 1991]. Elasticity problems are usually formulated either in terms of deformation parameters or stress parameters. Among the existing mathematical models of plane boundary value stress problems, the stress function approach and the displacement formulation are notable [Timoshenko and Goodier 1979]. Application of the stress function formulation in conjunction with the finite difference technique has been reported for the solution for plane elastic problems in which all boundary conditions are described in terms of stresses only [Chow et al. 1953; Chapel and Smith 1968]. Further, Conway [1953] extended the stress function formulation in the form of Fourier integrals to the case in which the material was orthotropic, and obtained analytical solutions for a number of ideal problems. The shortcomings of the stress function approach are that it accepts boundary conditions only

Keywords: orthotropic composite panel, displacement potential function, finite difference method, mixed boundary conditions, end moment, shear loading.

in terms of loadings. Boundary restraints that are specified in terms of displacement components cannot be satisfactorily imposed on the stress function. Because most practical problems of elasticity are of mixed boundary value type, the stress function approach fails to provide an explicit understanding of the state of stresses at the critical support and stiffener components. Here, a 'mixed boundary value problem' refers to one in which the displacement components are described over part of the boundary surface and the stress components over the remainder of the boundary surface. The boundary conditions may also be specified as a mixture of boundary restraints and boundary loadings, as realized in the cases of stiffeners, guided edges, etc.

Reliable and accurate prediction of stresses, especially at the surfaces of engineering structures, is of great importance with respect to reliability, safety, and economic design. The uncertainties associated with the prediction of surface stresses by standard computational approaches (for example, the finite element method, FEM) have been pointed out by several researchers [Richards and Daniels 1987; Smart 1987; Dow et al. 1990]. On the other hand, introducing a new boundary modeling approach for finite difference applications of the displacement formulation of solid mechanics [Dow et al. 1990] solved the problem of a uniformly loaded cantilever beam and reported that the accuracy of the finite difference method (FDM), with respect to reproducing the state of stresses along the bounding surfaces, was much higher than the accuracy of FE analysis. However, the computational efforts of the FD analysis, under the new boundary modeling approach, were somewhat greater than the efforts required for FE analysis. Recently, Ranzi et al. [2006] reported a comparative study of the performances of available modeling approaches for the analysis of composite beams with partial shear interactions. Comparing the performances with exact analytical solutions, the FDM was determined to be an adequate numerical tool for describing the composite behavior of beams, and the corresponding FD solutions were shown to be more accurate when compared with the usual eight degree-of-freedom FEM solutions, even when finer discretization was used for the FEM solutions.

The recent research and the developments with respect to using the displacement potential approach [Ahmed et al. 1996; 1998; 2005b; Akanda et al. 2002] have generated renewed interest in the fields of both analytical and numerical solutions for practical stress problems. In this boundary modeling approach, the plane elastic problem is formulated in terms of a potential function of space variables, defined in terms of two displacement components that must satisfy a single differential equation of equilibrium. Moreover, the present computational approach permits the reduction of the number of dependent variables that must be evaluated at each nodal point to one. This is an advantage over the standard solution methods, which use at least two unknowns at each nodal point for solving plane problems. As a result, the total number of simultaneous equations that must be solved in the present approach is reduced to half of those required in usual approaches, which eventually leads to a drastic reduction in computational effort as well as increased overall accuracy of the solution [Ahmed et al. 2005a]. The present modeling approach also enables us to very efficiently manage the mixed mode of boundary conditions as well as their zones of transition. Recently, Ahmed et al. [2005a] proposed a general displacement potential formulation for the solution for anisotropic composite structures. Further, Nath *et al.* extended the use of the formulation to the problems of orthotropic composite materials, and obtained analytical solutions for a number of composite structures under various types of loading and supporting conditions [Nath et al. 2006; 2007; 2009].

A new analysis of the elastic field of composite panels subjected to an end moment as well as a shear loading is the subject of the present paper. The panels are assumed to be rigidly fixed at one end,

and the fibers are situated along the longitudinal axis of the panel. The solutions are obtained using the displacement potential formulation in conjunction with FDM, and the corresponding distributions of stress and displacements are presented mainly in the form of graphs as well as the predicted deformed shape. Some of the issues of interest, for example, the effects of the aspect ratio, edge stiffening, and fiber reinforcement, etc. on the elastic field are also investigated. Finally, a comprehensive comparative analysis is presented in an attempt to check the appropriateness as well as superiority of the present numerical solutions. More specifically, the reliable prediction of stresses at the critical sections of the panel, especially at the regions of transition between physical conditions, is discussed in comparison to the stresses predicted by standard FEM.

2. Displacement potential formulation

The two differential equations for equilibrium in plane stress problems describing orthotropic elastic bodies of Hookean materials, with respect to a rectangular coordinate system, in the absence of body forces, and in terms of the displacement components, are as follows [Jones 1975; Timoshenko and Goodier 1979]:

$$\left(\frac{E_1^2}{E_1 - \nu_{12}^2 E_2}\right) \frac{\partial^2 u_x}{\partial x^2} + \left(\frac{\nu_{12} E_1 E_2}{E_1 - \nu_{12}^2 E_2} + G_{12}\right) \frac{\partial^2 u_y}{\partial x \partial y} + G_{12} \frac{\partial^2 u_x}{\partial y^2} = 0, \tag{1}$$

$$\left(\frac{E_1 E_2}{E_1 - \nu_{12}^2 E_2}\right) \frac{\partial^2 u_y}{\partial y^2} + \left(\frac{\nu_{12} E_1 E_2}{E_1 - \nu_{12}^2 E_2} + G_{12}\right) \frac{\partial^2 u_x}{\partial x \partial y} + G_{12} \frac{\partial^2 u_y}{\partial x^2} = 0, \tag{2}$$

where E_1 and E_2 are the elastic moduli of the material in the x - and y -directions, respectively, ν_{12} is the major Poisson’s ratio, and G_{12} is the in-plane shear modulus. Instead of solving the above two elliptic partial differential equations simultaneously, the existence of a new potential function of space variables is investigated in an attempt to reduce the problem to the determination of a single variable from a single differential equation of equilibrium. In the present approach, a new potential function $\psi(x, y)$ is thus defined in terms of the two displacement components as follows [Ahmed et al. 2005a]:

$$u_x = \alpha_1 \frac{\partial^2 \psi}{\partial x^2} + \alpha_2 \frac{\partial^2 \psi}{\partial x \partial y} + \alpha_3 \frac{\partial^2 \psi}{\partial y^2}, \quad u_y = \alpha_4 \frac{\partial^2 \psi}{\partial x^2} + \alpha_5 \frac{\partial^2 \psi}{\partial x \partial y} + \alpha_6 \frac{\partial^2 \psi}{\partial y^2}. \tag{3}$$

Here, the α s are unknown material constants. For a unidirectional orthotropic composite lamina, in which the fibers are directed along the x -axis, the values of these constants are

$$\alpha_1 = \alpha_3 = \alpha_5 = 0, \quad \alpha_2 = 1, \quad \alpha_4 = -\frac{E_1^2}{Z_{11}}, \quad \alpha_6 = -\frac{G_{12}(E_1 - \nu_{12}^2 E_2)}{Z_{11}} \tag{4}$$

(see [Ahmed et al. 2005a]), where

$$Z_{11} = \nu_{12} E_1 E_2 + G_{12}(E_1 - \nu_{12}^2) E_2.$$

Substitution of (3) into the first equilibrium condition, (1), shows that the latter is automatically satisfied. Therefore, ψ must satisfy the second equilibrium condition, (2), only. Expressing (2) in terms of

the potential function ψ , for the case of orthotropic plane stress problems, ψ must satisfy the condition

$$E_1 G_{12} \frac{\partial^4 \psi}{\partial x^4} + E_2 (E_1 - 2\nu_{12} G_{12}) \frac{\partial^4 \psi}{\partial x^2 \partial y^2} + E_2 G_{12} \frac{\partial^4 \psi}{\partial y^4} = 0; \tag{5}$$

see [Ahmed et al. 2005a; Nath et al. 2007].

Because the present approach considers a single dependent variable for solving the panel problem, all of the equations associated with the normal and the tangential components of stress and displacement are expressed in terms of the function ψ . The expressions for the displacement components for the plane stress orthotropic composite materials are restated here:

$$u_x(x, y) = \frac{\partial^2 \psi}{\partial x \partial y}, \tag{6}$$

$$u_y(x, y) = -\frac{1}{Z_{11}} \left[E_1^2 \frac{\partial^2 \psi}{\partial x^2} + G_{12} (E_1 - \nu_{12}^2 E_2) \frac{\partial^2 \psi}{\partial y^2} \right]. \tag{7}$$

The differential equations associated with the stress components are obtained by substituting Equations (6) and (7) into the stress–displacement relations of plane stress problems. The resulting expressions for the stress components in terms of the function ψ are as follows [Ahmed et al. 2005a]:

$$\sigma_{xx}(x, y) = \frac{E_1 G_{12}}{Z_{11}} \left[E_1 \frac{\partial^3 \psi}{\partial x^2 \partial y} - \nu_{12} E_2 \frac{\partial^3 \psi}{\partial y^3} \right], \tag{8}$$

$$\sigma_{yy}(x, y) = \frac{E_1 E_2}{Z_{11}} \left[(\nu_{12} G_{12} - E_1) \frac{\partial^3 \psi}{\partial x^2 \partial y} - G_{12} \frac{\partial^3 \psi}{\partial y^3} \right], \tag{9}$$

$$\sigma_{xy}(x, y) = -\frac{E_1 G_{12}}{Z_{11}} \left[E_1 \frac{\partial^3 \psi}{\partial x^3} - \nu_{12} E_2 \frac{\partial^3 \psi}{\partial x \partial y^2} \right]. \tag{10}$$

3. Geometries and loadings of the panel

Two cases of an orthotropic panel are considered (Figure 1). Case I is a composite panel with a rectangular cross section that is supported at its left lateral end ($x/b = 0$) and subjected to a bending moment at its right lateral end ($x/b = 1$). The normal stress on the right lateral end, causing the bending moment,

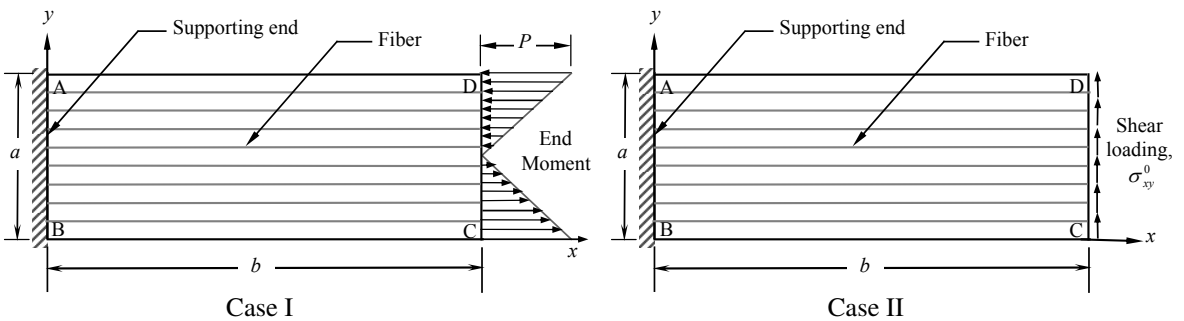


Figure 1. Model of orthotropic composite panels subjected to an end moment (Case I) or to shear loading (Case II).

is distributed according to a simple linear relationship given by $\sigma_n = P[1 - 2(y/a)]$, where P is the maximum intensity of the stress.

Case II is also a panel with a rectangular cross section that is supported at its left lateral end and is subjected to a uniform shear loading (intensity σ_{xy}^0) at the right lateral end. The supporting ends of the panels are considered to be rigidly fixed, and the fibers are assumed to be situated along the panel length. In both cases, b/a ratios of 1, 2, and 3 are considered.

4. Numerical solution to the problem

The FDM is used to discretize the governing differential equation (5) as well as the differential equations associated with the boundary conditions (6)–(10). The discrete values of the potential function $\psi(x, y)$, at the mesh points of the domain concerned, are solved from the system of linear algebraic equations resulting from the application of the governing equation and the boundary conditions by the use of a direct method of solution.

Discretization of the domain. The region of interest is divided into the desired number of mesh points, and the values of the dependent function $\psi(x, y)$ are sought only at these points. Depending upon the type of differential equations involved and on the geometry of the panel, a uniform rectangular mesh network is used. The error of the computational approach is of the order h^2 , and a mesh network of around 450 nodal points would be sufficient for an accurate and stable numerical solution [Akanda et al. 2000]. The discretization scheme of the panel is schematically illustrated in Figure 2. The governing differential equation, which is used to evaluate the function $\psi(x, y)$ only at the internal mesh points, is expressed in difference form using central difference operators as

$$\begin{aligned} F_1(\psi(i-2, j) + \psi(i+2, j)) - F_2(\psi(i-1, j) + \psi(i+1, j)) - F_3(\psi(i, j+1) + \psi(i, j-1)) \\ + F_4\psi(i, j) + F_5(\psi(i+1, j+1) + \psi(i+1, j-1) + \psi(i-1, j+1) + \psi(i-1, j-1)) \\ + F_6(\psi(i, j-2) + \psi(i, j+2)) = 0, \quad (11) \end{aligned}$$

where

$$\begin{aligned} F_1 = (k/h)^4, \quad F_2 = 4(k/h)^4 + 2M(k/h)^2, \quad F_3 = 2M(k/h)^2 + 4\frac{E_2}{E_1}, \\ F_4 = 6(k/h)^4 + 4M(k/h)^2 + 6\frac{E_2}{E_1}, \quad F_5 = M(k/h)^2, \quad F_6 = \frac{E_2}{E_1}, \quad M = \frac{E_2}{G_{12}} - \frac{2\nu_{12}E_2}{E_1}, \end{aligned}$$

Here h, k are the mesh lengths in the x - and y -directions, respectively.

The corresponding grid structure of the difference equation, Equation (11), for any internal mesh point (i, j) is shown in Figure 2. The pivotal point (i, j) in the grid structure is the point of application of the governing equation. As far as the present central-difference grid structure of the governing equation is concerned, when the point of application (i, j) becomes an immediate neighbor to the physical boundary, it will involve mesh points both interior and exterior to the physical boundary of the panel. Thus, an imaginary boundary, exterior to the physical boundary, as shown in Figure 2, is introduced such that the application of the governing equation (11), especially to the points in the immediate neighborhood of the

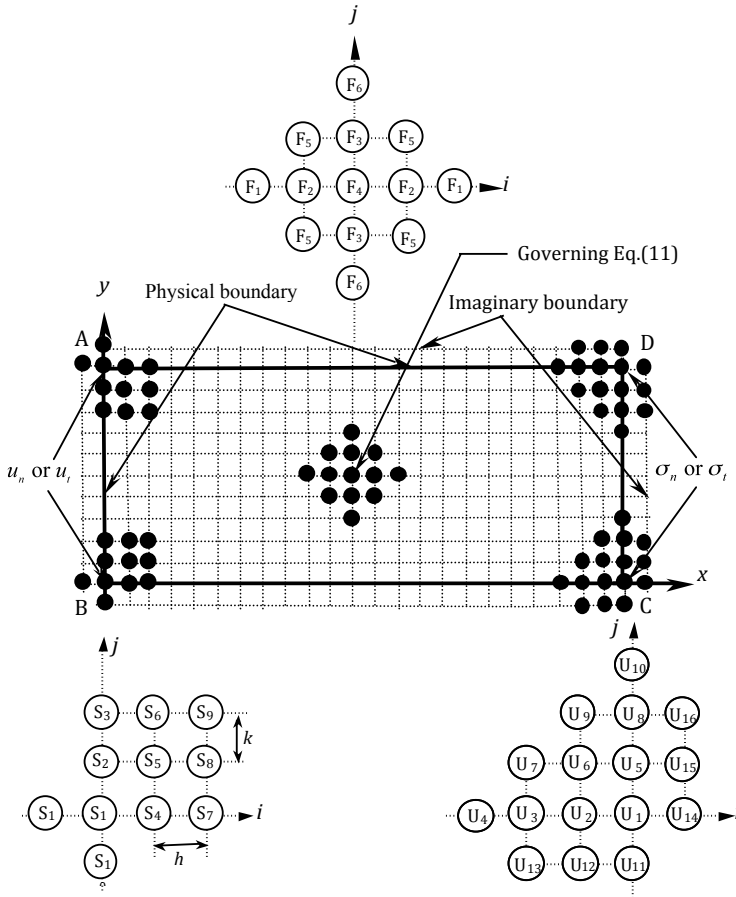


Figure 2. Finite-difference mesh network used to describe the panel, and the application of FD stencils of the governing equation and boundary conditions.

physical boundary, involves no points exterior to the model boundary (imaginary one), thereby causing no difficulties in developing a straightforward program.

Management of boundary conditions. The physical conditions at any point on a boundary are usually visualized in terms of normal and tangential components of displacement and stress. The expressions for the normal and tangential components of displacement in terms of the function ψ are

$$u_n(x, y) = lu_x(x, y) + mu_y(x, y), \quad u_t(x, y) = lu_y(x, y) - mu_x(x, y), \quad (12)$$

where l and m are the direction cosines of a point on the boundary. Similarly, the expressions for the normal and tangential components of stress for points on the body are

$$\sigma_n(x, y) = l^2\sigma_{xx}(x, y) + 2lm\sigma_{xy}(x, y) + m^2\sigma_{yy}(x, y), \quad (13)$$

$$\sigma_t(x, y) = (l^2 - m^2)\sigma_{xy}(x, y) + lm[\sigma_{yy}(x, y) - \sigma_{xx}(x, y)]. \quad (14)$$

Expressions (12)–(14) can be found in [Akanda et al. 2002].

Because the differential equations associated with the boundary conditions contain second and third order derivatives of the function ψ , the use of central difference expressions is not practical because most of the time it leads to the inclusion of points exterior to the imaginary boundary. The derivatives of the boundary expressions are thus replaced by their corresponding backward or forward difference formulas, keeping the order of the local truncation error the same, $O(h^2)$. In order to avoid the inclusion of points exterior to the imaginary boundary, four different sets of finite difference expressions for each of the boundary conditions are developed for the points at different regions of the boundary. These four sets of algebraic equations are derived by adopting different combinations of forward and backward difference schemes. The choice of the appropriate set of expressions for a point on the boundary is determined by the point's position on the boundary, which avoids the introduction of additional mesh points external to the imaginary boundary. Some of the difference equations derived for the boundary conditions are shown below.

For example, the finite difference form of the normal or tangential component of displacement (i -forward, j -forward) for the bottom left boundary is expressed as follows:

$$\begin{aligned} u_n(i, j) = & S_1\psi(i, j) + S_2\psi(i, j + 1) + S_3\psi(i, j + 2) \\ & + S_4\psi(i + 1, j) + S_5\psi(i + 1, j + 1) + S_6\psi(i + 1, j + 2) + S_7\psi(i + 2, j) \\ & + S_8\psi(i + 2, j + 1) + S_9\psi(i + 2, j + 2) + S_{10}\psi(i, j - 1) + S_{11}\psi(i - 1, j). \end{aligned} \quad (15)$$

Similarly, the finite difference form of the normal or tangential component of stress (i -backward, j -forward) for the bottom right boundary is expressed as follows:

$$\begin{aligned} \sigma_n(i, j) = & U_1\psi(i, j) + U_2\psi(i - 1, j) + U_3\psi(i - 2, j) + U_4\psi(i - 3, j) + U_5\psi(i, j + 1) \\ & + U_6\psi(i - 1, j + 1) + U_7\psi(i - 2, j + 1) + U_8\psi(i, j + 2) + U_9\psi(i - 1, j + 2) \\ & + U_{10}\psi(i, j + 3) + U_{11}\psi(i, j - 1) + U_{12}\psi(i - 1, j - 1) + U_{13}\psi(i - 2, j - 1) \\ & + U_{14}\psi(i + 1, j) + U_{15}\psi(i + 1, j + 1) + U_{16}\psi(i + 1, j + 2), \end{aligned} \quad (16)$$

where the coefficients S_i and U_i are functions of elastic constants, direction cosines, and mesh lengths. The corresponding FD grid structures of the difference equations, (15) and (16), are also shown in Figure 2. The structures of the normal and tangential components are found to be identical in form, but they differ in the sense of the nodal coefficients.

Placement of boundary conditions and evaluation of stresses and displacements. There are two conditions to be satisfied at a point on the physical boundary of the rectangular panel, therefore, two difference equations corresponding to the respective boundary conditions are applied to the same point on the boundary. Of these two equations, one is used to evaluate the function ψ at the physical boundary point, and the remaining equation is used to evaluate ψ at the corresponding point on the imaginary boundary. Special treatments are adopted for the four corner mesh points, which are generally the points of transition for the boundary conditions. The program is organized in such a fashion that it will satisfy three out of the available four boundary conditions for each corner point. As a result, the outer corner points of the imaginary boundary are not taken into consideration for the present solution, as illustrated in the FD mesh network

of Figure 2. Therefore, the application of the governing equation as well as the necessary boundary conditions ensures that every mesh point of the computational domain will have a single algebraic equation in terms of the function ψ for its evaluation. Finally, in order to evaluate the stress and displacement components, four sets of finite difference expressions for each of the displacement and stress components (6)–(10) are developed in a fashion similar to that adopted in the case of the boundary conditions. Because all of the stress and displacement components are expressed in terms of the function ψ , the parameters of interest are readily calculated from the ψ values obtained at the mesh points of the domain.

In the present computational approach, the number of algebraic equations is equal to the number of field nodal points, and for each nodal point, there is only one unknown. Thus an $(n \times n)$ matrix of coefficients is generated for a total of n active field nodal points. It was shown that the present displacement potential-based FDM can save a tremendous amount of computational effort (approximately 87%) for the solution for a two-dimensional problem in comparison with the effort required for the usual computational approaches [Ahmed et al. 2005a].

5. Results and discussion

The results of the finite difference solution for the composite panel subjected to two different types of loading, as described in Section 3, are presented in this section. The results are presented mainly in the form of the calculated deformed shape and the distribution of the various stress and displacement components of interest. In all cases, displacements are normalized with respect to panel width (a), and stresses are normalized with respect to the maximum intensity of the applied loading (P and σ_{xy}^0 , see Figure 1). The details of the boundary conditions used to obtain the FD solutions, as they relate to the bounding edges, are given in Table 1, while Table 2 presents the boundary conditions associated with the corner points. For most of the results, the panel material is considered to be a boron/epoxy composite for which the effective mechanical properties, together with the properties of glass/epoxy and graphite/epoxy, are listed in Table 3. For the panel subjected to the end moment (Case I), solutions are obtained for different panel aspect ratios (b/a). The solutions for the elastic field of the panel (Case II) are presented mainly in a comparative fashion with the corresponding FEM solutions. The magnitude of

boundary segment	given boundary conditions	correspondence between mesh points and given boundary conditions	
		mesh point on the physical boundary conditions	mesh point on the imaginary boundary conditions
AB	(u_n, u_t)	$u_n = 0$	$u_t = 0$
BC	(σ_n, σ_t)	$\sigma_n = 0$	$\sigma_t = 0$
DA	(σ_n, σ_t)	$\sigma_n = 0$	$\sigma_t = 0$
CD (Case I)	(σ_n, σ_t)	$\sigma_n = P[1 - 2(y/a)]$	$\sigma_t = 0$
CD (Case II)	(σ_n, σ_t)	$\sigma_t = \sigma_{xy}^0$	$\sigma_n = 0$

Table 1. Boundary conditions used for different boundary segments of the panels, Case I and Case II (see Figure 1).

corner points	given boundary conditions	used boundary conditions	correspondence between mesh points and given boundary conditions	
			mesh point on the physical boundary conditions	mesh point on the imaginary boundary conditions
A	$[(u_n, u_t), (\sigma_n, \sigma_t)]$	$[u_n, u_t, \sigma_n]$	$\sigma_n = 0$	$u_n = 0, u_t = 0$
B	$[(u_n, u_t), (\sigma_n, \sigma_t)]$	$[u_n, u_t, \sigma_n]$	$\sigma_n = 0$	$u_n = 0, u_t = 0$
C (Case II)	$[(\sigma_n, \sigma_t), (\sigma_n, \sigma_t)]$	$[\sigma_n, \sigma_t, \sigma_n]$	$\sigma_t = \sigma_{xy}^0$	$\sigma_n = 0, \sigma_t = 0$
C (Case I)	$[(\sigma_n, \sigma_t), (\sigma_n, \sigma_t)]$	$[\sigma_n, \sigma_t, \sigma_n]$	$\sigma_n = P$	$\sigma_n = 0, \sigma_t = 0$
D (Case II)	$[(\sigma_n, \sigma_t), (\sigma_n, \sigma_t)]$	$[\sigma_n, \sigma_t, \sigma_n]$	$\sigma_t = \sigma_{xy}^0$	$\sigma_n = 0, \sigma_t = 0$
D (Case I)	$[(\sigma_n, \sigma_t), (\sigma_n, \sigma_t)]$	$[\sigma_n, \sigma_t, \sigma_n]$	$\sigma_n = -P$	$\sigma_n = 0, \sigma_t = 0$

Table 2. Boundary conditions used for corner points of the panels, Case I and Case II (see Figure 1).

material	property	boron/epoxy	graphite/epoxy	glass/epoxy
composite	V_f	0.50	0.70	0.45
	E_1 (10^6 psi)	29.59	26.25	5.60
	E_2 (10^6 psi)	2.68	1.49	1.20
	G_{12} (10^6 psi)	0.81	1.04	0.60
	ν_{12}	0.23	0.28	0.26
epoxy	E (10^6 psi)	0.50		
	ν	0.35		

Table 3. Mechanical properties of composites used.

the maximum intensity of loading per unit area for the two cases of the panel (P and σ_{xy}^0 , respectively) is arbitrarily assumed to be 6000 psi (41.4 MPa). The FD mesh network used to model the panels with different aspect ratios contains nodal points ($24-56 \times 19$) in the direction of x and y , respectively.

5.1. Orthotropic panel under application of an end moment (Case I). The numerical results obtained for the relevant displacement and stress components at different sections of the panel under the end moment are analyzed and presented in this section. Figure 3, top, shows the predicted deformed shape of the boron/epoxy panel with $b/a = 2$, in which the displacements are magnified by a factor of 100. The overall deformation pattern of the panel is found to be in good agreement with the physical model of the panel. From the distribution of axial displacement components (u_x) at different longitudinal sections of a panel, it is observed that the displacement varies linearly and antisymmetrically with respect to the panel width. At the right lateral end, the displacement takes its highest value and decreases gradually towards the supporting end. For a particular longitudinal section, the lateral displacement (u_y) is found to remain constant over the panel width, the magnitude of which, however, gradually decreases as we move towards the supporting end. Furthermore, the displacement field of the orthotropic panel is analyzed in

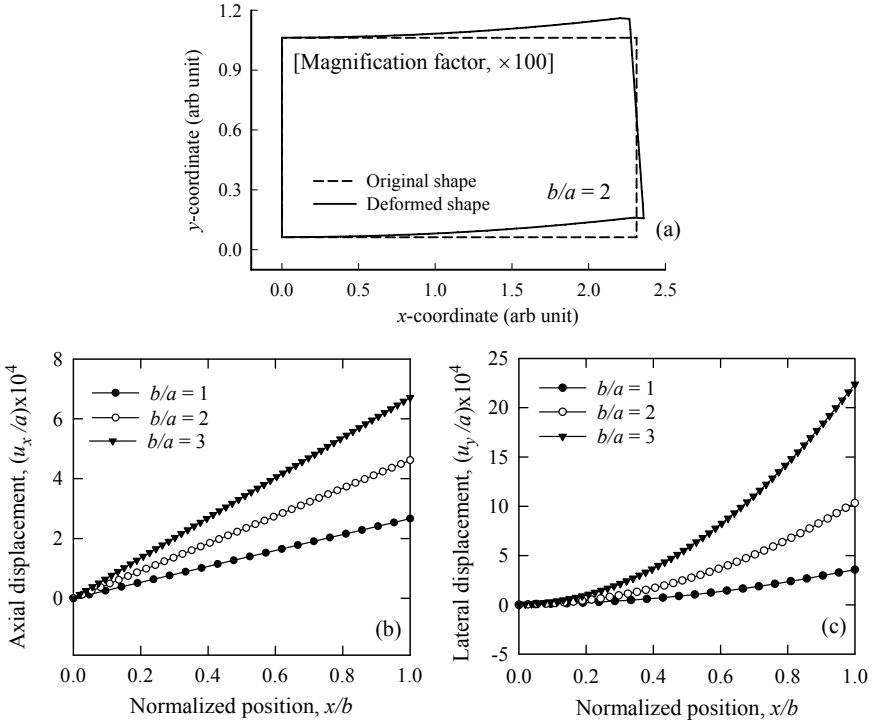


Figure 3. Deformed shape (top) and distributions of axial (bottom left) and lateral (bottom right) displacements at section $y/a = 0$ of boron/epoxy panels (Case I).

the perspective of panel aspect ratio. The axial and lateral displacements along the lower longitudinal edge ($y/a = 0$) of the panel are presented with respect to the normalized axial position, as a function of aspect ratio, in Figure 3, bottom. The axial displacement varies linearly with respect to the panel length, whereas the lateral displacement varies nonlinearly. As far as the magnitude is concerned, the lateral displacements are found to take much higher values than the axial displacements.

Figure 4 illustrates the distribution of axial stress components at different sections of the orthotropic

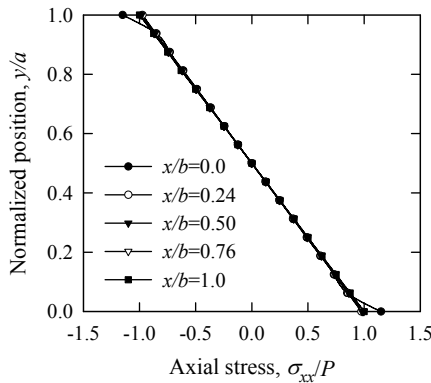


Figure 4. Distribution of the axial stress component at different sections of the boron/epoxy panel (Case I, $b/a = 2$).

panel, $b/a = 2$. It is observed from the solution that the distribution of axial stress is identical for all longitudinal sections of the panel, and varies linearly from its maximum to minimum value with respect to panel width. The maximum and minimum values of the normalized axial stress are found to occur at the two opposing edges, the magnitudes of which are 1 and -1 . As far as the applied moment loading is concerned, the FD solution for the axial stress component is completely in agreement with the expected solution, both in terms of magnitude and nature of variation. The axial stress distributions are found to be independent of the panel aspect ratio, that is, at a particular section of x/b , the distribution remains identical for different b/a ratios both in terms of magnitude and shape. Other components of stress are found to be insignificant when their magnitudes are compared with the magnitude of the axial stress.

5.2. Orthotropic panel subjected to shear loading (Case II). In this section, the FD solutions for the composite panel (Case II) are presented mainly in the form of a comparison with the corresponding solutions from the FEM. Note that no reliable theoretical solution for the present composite panel problem is available in the literature. The reliability and accuracy of the present numerical solutions is, therefore, verified by comparison with a numerical solution that is based on a completely different philosophy. Therefore, the same panel problem was solved by FEM using the standard commercial software ANSYS with two different aspect ratios, $b/a = 2$ and 3. Considering the rectangular shape of the panel, four-noded rectangular plane elements (orthotropic) are used to construct the corresponding mesh network. All elements have the same aspect ratio, and their distribution is kept uniform all over the domain. The total number of finite elements used to discretize the panel is 800 (40×20). The convergence as well as accuracy of the solution is verified by varying the element mesh density.

Figure 5 presents the distributions of displacement components at the mid-longitudinal section of the composite panels having different aspect ratios. For this particular loading on the panel, the lateral stress distributions at the mid-longitudinal section are found to be straight vertical lines when analyzed from the perspective of the panel width. The corresponding FE predictions of displacements are also included in the same graphs. In general, the two solutions for displacements are very close to each other. A critical comparison of the axial displacements reveals that the discrepancy between the two solutions is almost negligible for panels with higher aspect ratios, but for shorter panels, FEM predicts slightly higher displacements, especially in the regions near the two opposing longitudinal edges. Unlike the constant lateral

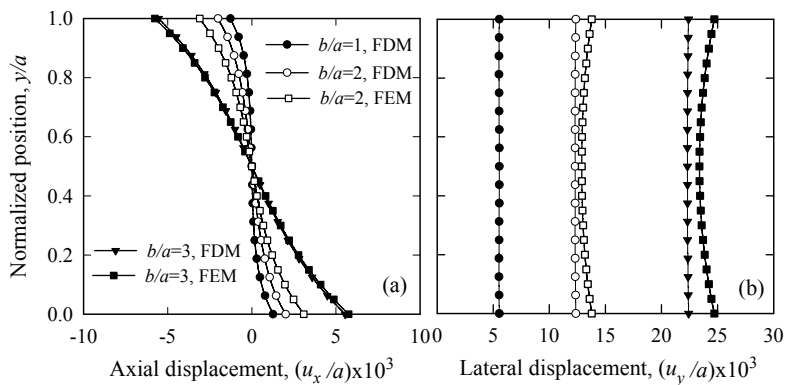


Figure 5. Distributions of (a) axial and (b) lateral displacements at section $x/b = 0.5$ of boron/epoxy panels (Case II).

displacements predicted by the present numerical approach, FEM predicts a nonlinear distribution of the displacement component, in which the case of axial displacement similarly shows a slight increase in lateral displacement in the neighborhood of the opposing longitudinal edges. As far as the physical characteristics of the panel are concerned, it may be difficult to verify that the FEM solution is reliable, especially around the two opposing longitudinal edges where the displacements are found to assume higher values than those at the interior region of the same section, $x/b = 0.5$. Results also show that the aspect ratio has a significant influence on the displacement field of an orthotropic panel subjected to a shear loading.

Figure 6 presents the axial stress distributions at the support, $x/b = 0$ and at section $x/b = 0.1$ of the panels for which $b/a = 2$ and 3. Along with the present FD solutions, the results of FEM are included for the convenience of direct comparison. Sections near the supporting end have been chosen here for consideration because the fixed end of the panel is identified to be the most critical section in terms of stresses. For both panels, the two numerical solutions for axial stress are in excellent agreement. Slight discrepancies between the solutions are observed, particularly at the corner points of the supporting end. For the corner points of the supporting end, which are, in fact, the points of singularity by design, FE results show higher nonlinearity, and, thus, a higher value of the axial stress compared to the nonlinearity of FD solutions. The FD predictions at the section $x/b = 0.1$ are found to be identical to those of FE solutions both at the edges and in the interior region. In general, the stress level is found to increase with increased aspect ratio, and the nonlinearity of the distribution decreases as the panel becomes longer.

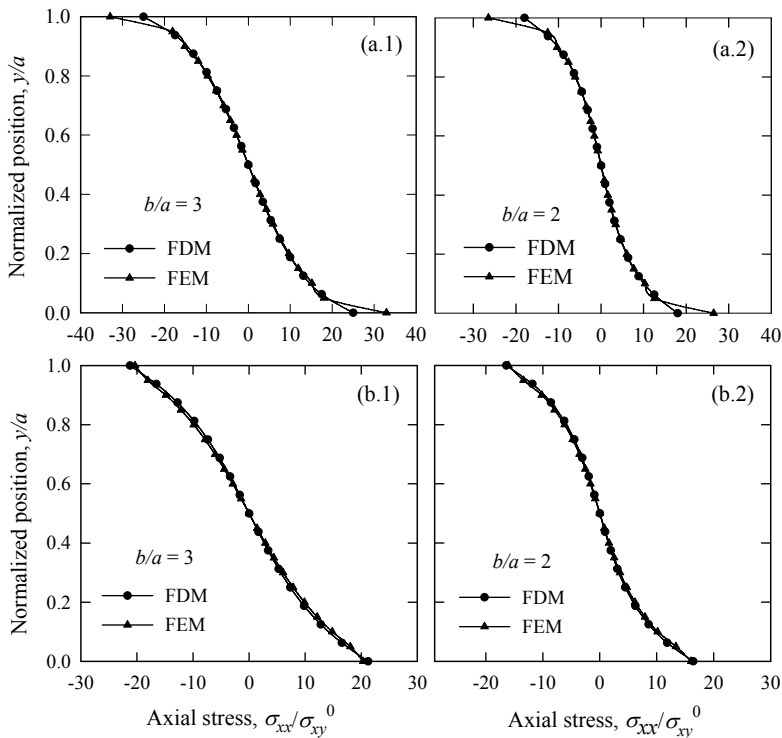


Figure 6. Distributions of the axial stress component at the supporting end (top row) and at the section $x/b = 0.1$ (bottom row) of boron/epoxy panels under shear loading (Case II).

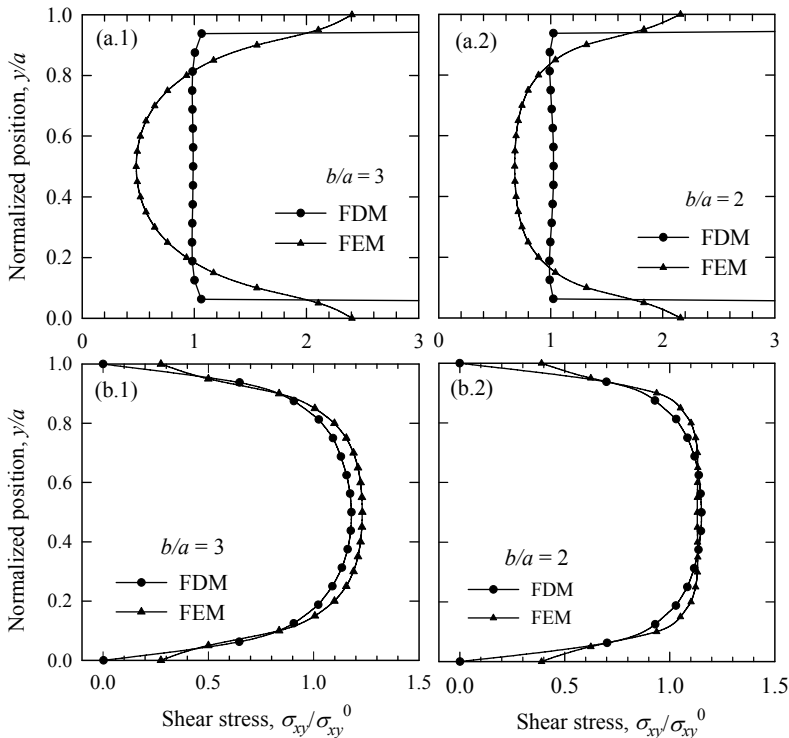


Figure 7. Distributions of the shear stress component at the supporting end (top row) and at the section $x/b = 0.1$ (bottom row) of boron/epoxy panels under shear loading (Case II).

The nonlinear distribution of the stress at the support is found to approach linearity as the section under consideration is moved away from the supporting end.

The distributions of shear stress along the panel width, particularly for sections $x/b = 0$ and 0.1 , are shown in Figure 7 for the panels with $b/a = 2$ and 3 . The corresponding FE predictions of shear stress are also included in the same figures. The top row of Figure 7 compares the two solutions for the shear stress at the supporting edges of the two panels $b/a = 2$ and 3 . The two solutions for the shear stress at the fixed support are found to differ quite substantially in terms of both magnitude and shape. The present ψ -formulation predicts a constant shear stress at the supporting end, the associated magnitude of which is found to be identical to that applied at the right lateral end. In addition, for the present orthotropic panel under shear loading, the shear stress at the support is found to be independent of panel aspect ratio. However, the FEM predicts a highly nonlinear distribution for the shear stress at the support. The maximum stress is observed at the upper and lower corners of the support, whereas the mid-region experiences the minimum stress. This particular shape of the distribution is found to be the reverse of the distributions obtained for the remaining longitudinal sections of the panel, in which the maximum stress is observed at the mid-region and the stress vanishes at the upper and lower edges. The effect of the singularity at the two corner points of the support is clearly reflected in the solutions from the FDM, because the stresses predicted at the two corner points are found to be higher than those at the remaining points of the support. Because the modeling of the boundary conditions for the corner points

in standard FE simulations does not take into account the effect of the singularity, the predictions near the corner regions may be unreliable. On the other hand, the transition of the boundary conditions in our FD modeling is handled in a more efficient way; for example, for each of the corner points of the panel, a total of three conditions out of the available four are satisfied appropriately (see Table 2). As a result, the present solutions are claimed to be closer to the actual states of the stresses. Note that the effect of the singularity in our FD solution is found to be highly localized, because the uniformity of the shear stress distribution at the supporting end remains unaffected except for the two corner points; see Figure 7, top. For sections away from the support, the shear stress distributions are significantly different from the distributions at the support, where the maximum stress at a particular section develops at the mid-width position, and the stress vanishes at the opposing longitudinal edges. The solutions at section $x/b = 0.1$ are presented in the bottom row of Figure 7. The two numerical solutions are found to be almost identical except for the small discrepancies at the two longitudinal surfaces. More specifically, the comparison of solutions in these two graphs shows that the FEM predictions of shear stress at the upper and lower surfaces are not reliable, even though the section concerned is free from singularities. The present FDM is, however, found to be free from the drawbacks of standard computational methods, and is able to predict the actual state of stresses at the surfaces.

Figure 8 shows the distribution of the lateral stress σ_{yy} at the sections $x/b = 0$ and 0.1 of the panel with different aspect ratios. Figure 8, top left, shows the solutions from the FDM at the supporting end

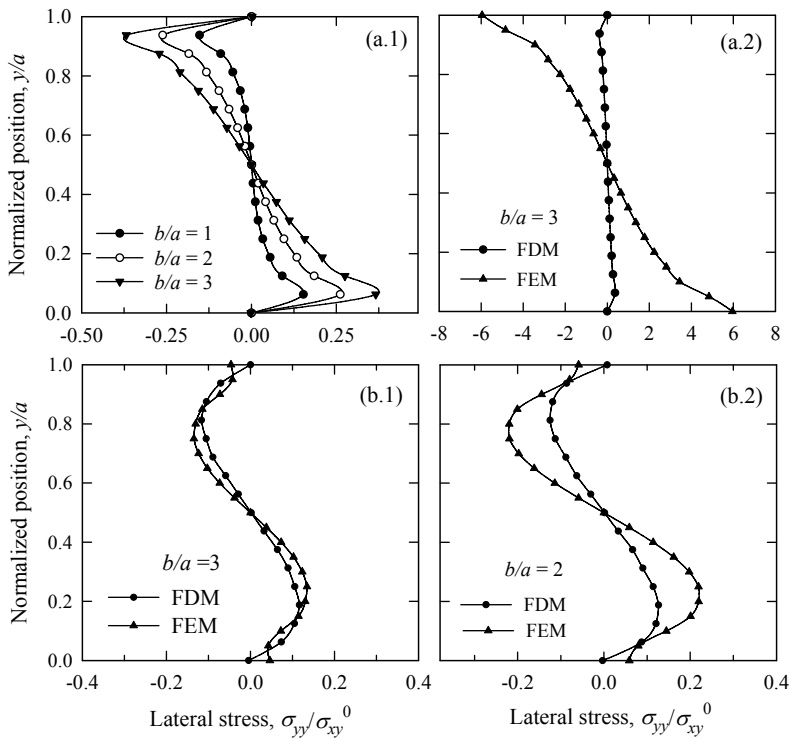


Figure 8. Distributions of the lateral stress component at the supporting end (top row) and at the section $x/b = 0.1$ (bottom row) of boron/epoxy panels under shear loading (Case II).

of the panels having $b/a = 1, 2,$ and 3 . Stresses at the support are found to increase with increasing panel aspect ratio, although the magnitude of the stress is lowest, compared to the magnitudes of shear and axial stresses, at the support. Stresses at the two corner points of the supporting end are found to be zero, which agrees with the physical conditions of the panels (see Table 2). Figure 8, top right, compares the solutions for the stress at the support obtained by FDM and FEM. As shown in the figure, the two solutions differ quite significantly from each other. The maximum normal stress at the support of the panel, $b/a = 3$, predicted by FEM, is found to be around 15 times higher than that predicted by FDM, which is in contrast with the stresses predicted for other sections of the panel. The bottom row of Figure 8 compares the solutions at section $x/b = 0.1$ for the two panels. From the figure, the two solutions at section $x/b = 0.1$ are found to be comparable with minor deviations, especially in the regions of the top and bottom surfaces. The FE solution for σ_{yy} does not reflect the physical characteristics of the panel, because the stresses do not vanish on the top and bottom surfaces, even when the section concerned is free from singularities. This inaccuracy of the FEM solution is found to be more pronounced as we approach the section containing the points of singularity, calling into question the reliability of the solution at the supporting end. The FD solution for the lateral stress σ_{yy} conforms appropriately to the physical model of the panel for all regions of interest at or away from the surfaces.

The superiority of the present FDM in reproducing the stresses at the bounding surfaces is further illustrated in Figure 9. The figure describes the distributions of axial stresses obtained by FDM and FEM at the right lateral end of the panel with $b/a = 2$, subjected to a uniform shear loading only. The boundary is basically free from any normal loading, and the corresponding state of stress is modeled exactly by the present method. However, the FEM solution is found to assume a peculiar antisymmetric distribution of the axial stress at the right end, which is highly unlikely. The effect of the singularity on the FEM solution is very prominent; quantitative analysis shows that the region over which the effect of singularity is prominent is more than 20% of the width, from both surfaces $y/a = 0$ and 1 . On the other hand, the present computational method allows one to exactly satisfy the condition that $\sigma_n = 0$ at the corner points of the right end (see Table 2), and, additionally, the condition is reflected appropriately in the solution.

The present computational scheme is extended to investigate the effects of stiffeners on the elastic field of the orthotropic panels. A maximum in the panel's axial stress (Case II) develops at the fixed support ($y/a = 0$) when the panel is free from the stiffeners. However, the stress at the support is found to vanish

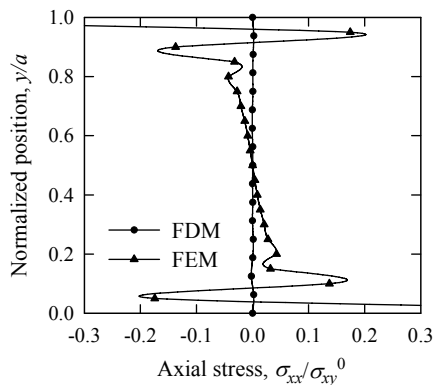


Figure 9. Comparison of two solutions for the axial stress distribution at the right lateral end of boron/epoxy panel ($b/a = 2$) under shear loading (Case II).

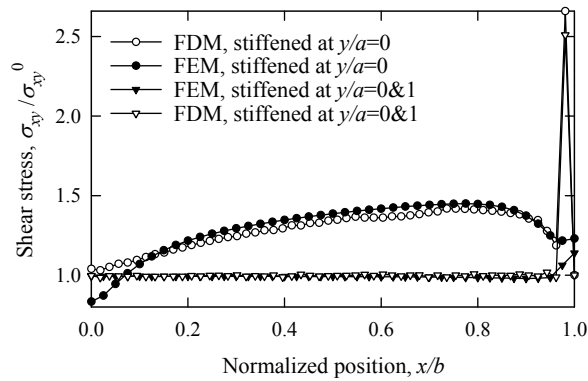


Figure 10. Distributions of the shear stress component along the stiffened edge, $y/a = 0$, of the boron/epoxy panel ($b/a = 3$) under shear loading (Case II).

when both opposing longitudinal edges ($y/a = 0$ and 1) are stiffened. We note that the physical condition of the stiffeners is modeled here by restraining the tangential displacements (u_x) of the longitudinal edges, while they are kept free from normal loading [Nath and Ahmed 2009]. The greatest impact of the stiffeners on the elastic field is realized in the shearing stress that develops along the stiffened edges, which is presented comparatively in Figure 10. The figure shows results for two cases of stiffened panels: (a) one of the longitudinal edges ($y/a = 0$) is stiffened; and (b) both longitudinal edges ($y/a = 0$ and 1) are stiffened. When the two opposing edges are stiffened, a uniform shearing stress develops along the stiffened edges, which is, with respect to magnitude, identical to the magnitude of the applied loading, σ_{xy}^0 . However, when only the edge, $y/a = 0$, is stiffened, a gradually increasing shearing stress is observed along the edge, the magnitude of which varies approximately within $1.0 \leq (\sigma_{xy}/\sigma_{xy}^0) < 1.5$ (see Figure 10). Similar to the previous cases, the FDM and FEM solutions are found to be nearly identical for almost all regions, except for the two extreme regions of the longitudinal edge. The maximum shearing stress predicted by the present FDM at the stiffened edge is $[\sigma_{xy}]_{\max} \approx 2.6\sigma_{xy}^0$, which is found on the stiffened edge immediately adjacent to the bottom-right corner; the corresponding FEM prediction is only 1.23 times the applied stress, σ_{xy}^0 , which is found at the bottom-right corner of the stiffened edge. Because the point of maximum stress, identified by the present FDM, is free from singularities, and, additionally, the method reproduces the stress at the bottom corner point of the right lateral end exactly, the FD prediction of the maximum shear stress appears to be highly reliable, even though it is not supported by FEM. Moreover, the stress predicted by FEM near the left corner region of the stiffened edge is questionable, because it assumes a value less than that of the applied one, σ_{xy}^0 .

Figure 11 presents the distribution of the lateral stress component at the fixed support of a panel composed of different composites. The distribution, therefore, describes the effect of fiber reinforcement in epoxy resin on the elastic field that develops under shear loading (Case II). The analysis presented shows that the effect of fiber reinforcement on the lateral stress, especially at the supporting end, is quite significant, whereas the effect on the axial and shearing stresses is not significant. Figure 11 reveals that the highest lateral stress develops when the epoxy resin is free from fibers, that is, the panel is composed of an isotropic epoxy resin. The stress level is found to decrease significantly as the longitudinal fibers are inserted into the resin. Among the composites, the maximum lateral stress at the support is found for the case of glass/epoxy. The general trend of the results suggests that at the supporting end of the shear

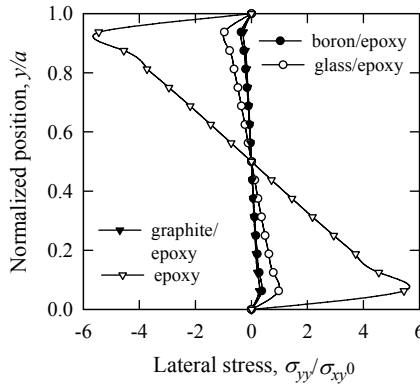


Figure 11. Effect of fiber reinforcement on the lateral stress at the supporting end of the boron/epoxy panel ($b/a = 3$) under shear loading (Case II).

loaded panel, where displacements in both directions are restrained, the magnitude of the lateral stress decreases with increased elastic moduli of the panel material (see Table 3).

6. Conclusions

The elastic behavior of an orthotropic composite panel with mixed boundary conditions is analyzed using an efficient numerical method. The special advantages of the method over existing approaches are its ability to satisfy and reproduce the boundary conditions appropriately, whether they are specified in terms of loading, restraints, or any combination thereof. Moreover, the present displacement potential-based computational method requires less computational effort to solve a problem compared to the effort required by standard computational approaches. Results of the present analysis show that critical stresses at the panel support are significantly influenced by the aspect ratio as well as edge stiffening, particularly when the panel is subjected to shear loading. Comparative analysis to the standard finite element method verifies the superiority of the present displacement potential formulation in conjunction with the finite difference method for predicting accurate and reliable stresses at any critical section of the panel, specially at the regions of transition of boundary conditions.

Index of notation

E_1	Elastic modulus of the material in x -direction	σ_{xx}, σ_{yy}	Axial and lateral stress components
E_2	Elastic modulus of the material in y -direction	σ_{xy}	Shearing stress component in the xy plane
ν_{12}, ν_{21}	Major and minor Poisson's ratios	u_n, u_t	Normal and tangential displacement
G_{12}	In-plane shear modulus in the 1-2 plane	σ_n, σ_t	Normal and tangential stress
E	Elastic modulus of isotropic material	ψ	Displacement potential function
G	Shear modulus of isotropic material	a, b	Dimensions of the panel in x - and y -directions
l, m	Direction cosines of the normal to a boundary	P	Maximum intensity of normal stress in Case I
u_x, u_y	Displacement components	σ_{xy}^0	Intensity of applied shear stress in Case II

References

[Ahmed et al. 1996] S. R. Ahmed, A. B. M. Idris, and M. W. Uddin, "Numerical solution of both ends fixed deep beams", *Comput. Struct.* **61**:1 (1996), 21–29.

- [Ahmed et al. 1998] S. R. Ahmed, M. R. Khan, K. M. S. Islam, and M. W. Uddin, “Investigation of stresses at the fixed end of deep cantilever beams”, *Comput. Struct.* **69**:3 (1998), 329–338.
- [Ahmed et al. 2005a] S. R. Ahmed, M. Z. Hossain, and M. W. Uddin, “A general mathematical formulation for finite-difference solution of mixed-boundary-value problems of anisotropic materials”, *Comput. Struct.* **83**:1 (2005), 35–51.
- [Ahmed et al. 2005b] S. R. Ahmed, S. K. D. Nath, and M. W. Uddin, “Optimum shapes of tire-treads for avoiding lateral slippage between tires and roads”, *Int. J. Numer. Methods Eng.* **64**:6 (2005), 729–750.
- [Akanda et al. 2000] M. A. S. Akanda, S. R. Ahmed, M. R. Khan, and M. W. Uddin, “A finite-difference scheme for mixed boundary-value problems of arbitrary-shaped elastic bodies”, *Adv. Eng. Software* **31**:3 (2000), 173–184.
- [Akanda et al. 2002] M. A. S. Akanda, S. R. Ahmed, and M. W. Uddin, “Stress analysis of gear teeth using displacement potential function and finite differences”, *Int. J. Numer. Methods Eng.* **53**:7 (2002), 1629–1640.
- [Chapel and Smith 1968] R. E. Chapel and H. W. Smith, “Finite-difference solutions for plane stresses”, *AIAA J.* **6**:6 (1968), 1156–1157.
- [Chow et al. 1953] L. Chow, H. D. Conway, and G. Winter, “Stresses in deep beams”, *Trans. ASCE* **118**:2557 (1953), 686–708.
- [Conway 1953] H. D. Conway, “Some problems of orthotropic plane stress”, *J. Appl. Mech. (ASME)* **20**:1 (1953), 72–76.
- [Conway et al. 1951] H. D. Conway, L. Chow, and G. W. Morgan, “Analysis of deep beams”, *J. Appl. Mech. (ASME)* **18** (1951), 163–172.
- [Dow et al. 1990] J. O. Dow, M. S. Jones, and S. A. Harwood, “A new approach to boundary modelling for finite difference applications in solid mechanics”, *Int. J. Numer. Methods Eng.* **30**:1 (1990), 99–113.
- [Durelli and Ranganayakamma 1989] A. J. Durelli and B. Ranganayakamma, “Parametric solution of stresses in beams”, *J. Eng. Mech. (ASCE)* **115**:2 (1989), 401–414.
- [Hardy and Pipelzadeh 1991] S. J. Hardy and M. K. Pipelzadeh, “Static analysis of short beams”, *J. Strain Anal. Eng. Des.* **26**:1 (1991), 15–29.
- [Jones 1975] R. M. Jones, *Mechanics of composite materials*, McGraw-Hill, New York, 1975.
- [Krishna Murty 1984] A. V. Krishna Murty, “Towards a consistent beam theory”, *AIAA J.* **22**:6 (1984), 811–816.
- [Nath and Ahmed 2009] S. K. D. Nath and S. R. Ahmed, “Displacement potential solution of stiffened composite struts subjected to eccentric loading”, *Appl. Math. Model.* **33**:3 (2009), 1761–1775.
- [Nath et al. 2006] S. K. D. Nath, S. R. Ahmed, and A. M. Afsar, “Displacement potential solution of short stiffened flat composite bars under axial loadings”, *Int. J. Appl. Mech. Eng.* **11**:3 (2006), 557–575.
- [Nath et al. 2007] S. K. D. Nath, A. M. Afsar, and S. R. Ahmed, “Displacement potential solution of a deep stiffened cantilever beam of orthotropic composite material”, *J. Strain Anal. Eng. Des.* **42**:7 (2007), 529–541.
- [Ranzi et al. 2006] G. Ranzi, F. Gara, G. Leoni, and M. A. Bradford, “Analysis of composite beams with partial shear interaction using available modelling techniques: a comparative study”, *Comput. Struct.* **84**:13–14 (2006), 930–941.
- [Richards and Daniels 1987] T. H. Richards and M. J. Daniels, “Enhancing finite element surface stress predictions: a semi-analytic technique for axisymmetric solids”, *J. Strain Anal. Eng. Des.* **22**:2 (1987), 75–86.
- [Smart 1987] J. Smart, “On the determination of boundary stresses in finite elements”, *J. Strain Anal. Eng. Des.* **22**:2 (1987), 87–96.
- [Suzuki 1986] S. Suzuki, “Stress analysis of short beams”, *AIAA J.* **24**:8 (1986), 1396–1398.
- [Timoshenko and Goodier 1979] S. Timoshenko and V. N. Goodier, *Theory of elasticity*, 3rd ed., McGraw-Hill, New York, 1979.

Received 15 Aug 2008. Revised 22 Jan 2009. Accepted 7 May 2009.

S. K. DEB NATH: sankar_20005@yahoo.com

Department of Mechanical Engineering, International University of Business, Agriculture and Technology, Dhaka-1230, Bangladesh

S. REAZ AHMED: reaz207@yahoo.com

Department of Mechanical Engineering, Bangladesh University of Engineering and Technology, BUET, Dhaka-1000, Bangladesh